*energies*

MDPI

*Article*

# Mechanical and Thermal Properties of 3D Printed Polycarbonate

**Anis Bahar** [1,2,3], **Sofiane Belhabib** [1], **Sofiane Guessasma** [2,*], **Ferhat Benmahiddine** [3], **Ameur El Amine Hamami** [3] and **Rafik Belarbi** [3,*]

1  Oniris, GEPEA, UMR 6144, CNRS-Nantes Université, F-44000 Nantes, France;
anis.bahar@univ-nantes.fr (A.B.); sofiane.belhabib@univ-nantes.fr (S.B.)
2  INRAE, UR1268 Biopolymères Interactions Assemblages, F-44300 Nantes, France
3  LaSIE, UMR 7356 CNRS-La Rochelle Université, Avenue Michel Crépeau, CEDEX 01,
F-17042 La Rochelle, France; ferhat.benmahiddine1@univ-lr.fr (F.B.); ahamami@univ-lr.fr (A.E.A.H.)
*  Correspondence: sofiane.guessasma@inrae.fr (S.G.); rbelarbi@univ-lr.fr (R.B.)

**Abstract:** This study aims at showing the potential of additive manufacturing as a new processing route for designing future insulators in the building sector. Polycarbonate (PC) is studied as a possible candidate for designing these new insulators. This polymer offers several advantages, among them fire resistance and stability of its physical properties at high temperatures. The 3D printing of PC is attempted using fused deposition modelling technology. The printing temperature and infill rate are varied to achieve optimal mechanical and thermal characteristics. The results show that an optimal printing temperature of 280 °C is needed to achieve high tensile performance. In addition, thermal properties including thermal conductivity and effusivity increase with the increase of the infill rate in opposition to the thermal diffusivity decrease.

**Keywords:** fused deposition modelling; polycarbonate; tensile properties; thermal properties; printing temperature

## 1. Introduction

Poorly insulated buildings are known to be a major source of huge energy consumption including heating and cooling [1]. Choosing adequate insulation has thus been made mandatory in recent legislation. For instance, The Energy Performance of Buildings Directive (EPBD) set by the European Union is meant to improve the energy performance of buildings in Europe [2]. Intensive work has been carried out recently in order to develop new and more efficient and environmentally friendly materials to be used in the field of insulation [3,4].

An interesting method of improving the insolation capabilities of a building is to design new insulators with local control of material architecture allowing, for instance, to adapt the shape, connectivity and local content of porosities [5–8]. Finite element computations are well suited for exploring new material designs [9]. The design of insulators with complex material architecture is, however, difficult to address by conventional manufacturing processes such as moulding or foaming. With the recent development of additive manufacturing (AM) technology, there is a strong tendency to rethink the material design based on required part functionality using a layer-by-layer deposition approach. This can be a game-changer for future building insulation. Indeed, AM is a promising new solution in the sustainable building sector, more particularly for developing biosourced polymeric solutions for the new generation of insulators. With a combination of computer-based control and a local deposition process, AM responds optimally to insulation requirements in the context of energy-saving policies being adopted worldwide.

However, there are challenges that face AM in the building sector. The potential of the printed parts at a large scale would be undermined by the large time needed to reach

production at the industrial level. In order to ensure the viability of AM technology on a large scale, several successful attempts have been made both at the laboratory scale and at the industrial level. Because the printing speed remains a major limitation of 3D printing processes [10], several routes have been explored recently to overcome this issue, among which is the design of innovative deposition strategies such as nozzles that allow large filament deposition rates [11] and multi-nozzle systems [12]. A realistic strategy that is currently tested is to obtain a balance between resolution and part size. For prints on a centimetre scale, it makes sense to use nozzles as small as 0.4 mm. For large realizations as in the case of the building sector, nozzles that are used for instance in crafting are on the centimetre scale [13].

FDM (Fused Deposition Modelling) is one of the most widespread AM technologies [14,15]. FDM combines simplicity and cost-effectiveness for processing polymeric structures without further need for extra-tooling or post-processing of manufactured parts [16]. A large amount of work was carried out in recent decades to understand the mechanical and thermal properties of printed parts and their dependency on printing parameters such as the printing temperature and the slicing conditions [17–20].

The present study explores the use of FDM to achieve new insulators from polycarbonate (PC). This material is generally known to be a tough, transparent plastic material with outstanding strength, stiffness, and impact. PC maintains its rigidity up to 140 °C and toughness down to −20 °C. This material is also reputed to be a slow-burning polymer. It passes, for instance, several severe flammability tests when combined with a special flame retardant. In this study, optimal printing conditions are explored for this material with a focus on two main leverages: printing temperature ranging from 270 °C to 300 °C, and infill rate from 10% up to 100%. For these conditions, both the mechanical and thermal properties are determined and compared to standard insulation materials used in the building sector. Figure 1 shows the general scheme adopted in this study to achieve results on the mechanical and thermal properties of PC.
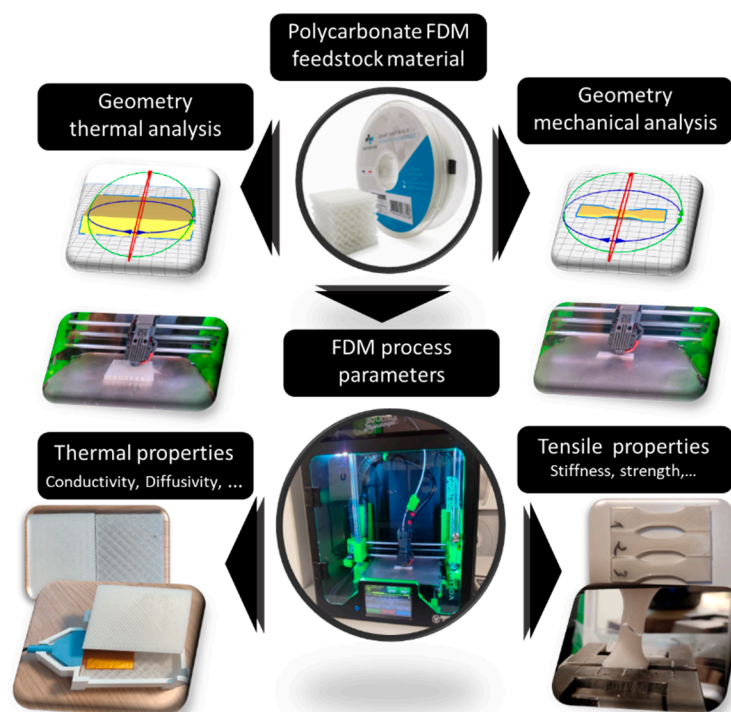


**Figure 1.** General scheme showing the methodology used to determine mechanical and thermal properties of PC.

## 2. Experimental Layout

A polycarbonate (PC) filament (diameter = 1.75 mm) from Nanovia company (Louargat, France) is used as a feedstock material for FDM. The main characteristics and printing conditions are given in Table 1.

**Table 1.** Recommended printing conditions and properties of PC feedstock materials.

| Category | Characteristics | Value |
|---|---|---|
| Mechanical properties | Density, (g/cm$^3$) | 1.13 g/cm$^3$ (ASTM D792) |
| | Tensile modulus | 700 MPa (ISO 527) |
| | Flexual modulus | 2000 MPa (ISO 178) |
| | Elongation at break | 120% (ISO 527) |
| | IZOD [1] impact testing (notched) | 65 kJ/m$^2$ |
| Thermal properties | MFI [1] | 10 g/10 min (300 °C, 1.2 kg/D1238) |
| | HDT [2] | 144 °C (D648 @ 4.6 kg/cm$^2$), 50 °C (D648 @ 18.6 kg/cm$^2$) |
| | Thermal expansion | $5.5 \times 10^{-5}$ mm/mm/°C (D696) |
| | Flammability | V-0 UL 94 @ 3.0 mm |
| | Fusion T° | 300 °C |
| | Tg | 120 °C |
| Electric properties | Resistivity volume | $4 \times 10^{16}$ Ω·cm (D257) |
| | Dielectric strength | 2.80 D150 |
| | Dissipation factor | 0.0082 D150 |
| | ARC resistance | 120 s |
| Recommended printing conditions | Extrusion T° | 260–290 °C |
| | Plate T° | 100–140 °C |
| | Enclosure T° | >100 °C |
| | Nozzle | All |
| | Printing Speed | 20–60 mm/s |
| | Diameter | 1.75 & 2.85 mm ± 50 μm |
| | Warping | 0.5 to 0.7% |
| | Humidity abs. | 0.15% (D570) |
| | Linear weight | 2.73 @ Ø 1.75 mm 7.23 @ Ø 2.85 mm |
| | Colours | Translucid, white, black |

[1] Melt Flow Index, [2] Heat Deflection Temperature.

The FDM process is performed using the Volumic stream 30 Ultra printer from Volumic 3D [21] (Nice, France) with a printer volume of 290 × 200 × 300 mm, and an extruder reaching 420 °C and a building platform heating up to 150 °C. The fixed printing conditions are described in Table 2. For mechanical testing of filament intrinsic properties, the as-received filament of a typical length of 80 mm was used with a gauge length of 40 mm (Table 2).

**Table 2.** Printing setting for PC filament.

| Parameter | Value |
|---|---|
| Sample dimensions (cm) | 80 × 20 × 4 mm (dogbone sample) |
| | 100 × 75 × 20 mm (thermal conductivity) |
| | 40 × 1.75 mm (filament) |
| Infill | 100% (mechanical testing) |
| | 10%, 30% (thermal conductivity) |
| Layer height | 0.2 mm |
| Wall thickness | 0.8 mm |
| Top/Bottom thickness | 1.0 mm |
| Printing speed | 50 mm/s |
| Printing temperature | 270 °C, 280 °C, 290 °C, 300 °C |
| Bed temperature | 110 °C |
| Building sequence | +45°/−45° |

Specific shapes were adopted to perform mechanical and thermal analyses which obey the standards. For mechanical testing, gthe eometry of the specimens was adapted according to the ISO 527-1/-2 and ASTM D638 sample type I standards [22]. These are dogbone shapes used for tensile testing of 3D printed PC samples. The overall length of the sample was adapted to the FDM printing process to avoid adhesion problems to the printing platform noticed on larger samples. In addition, parallelepipedic samples were used for thermal conductivity with 2 infill conditions (Table 2). As PC 3D printing requires particular heating conditions, both building platform $T_B$ and printing $T_P$ temperatures were adjusted to obtain successful prints without warpage or platform decohesion, which were the most challenging issues for high Tg materials such as PC. Preliminary tests demonstrated that $T_P$ of 260 °C does not allow successful prints although this is recommended by the supplier (Table 1). Illustrations of the sample geometries and layups (−45°/+45°) are shown in Figure 2.
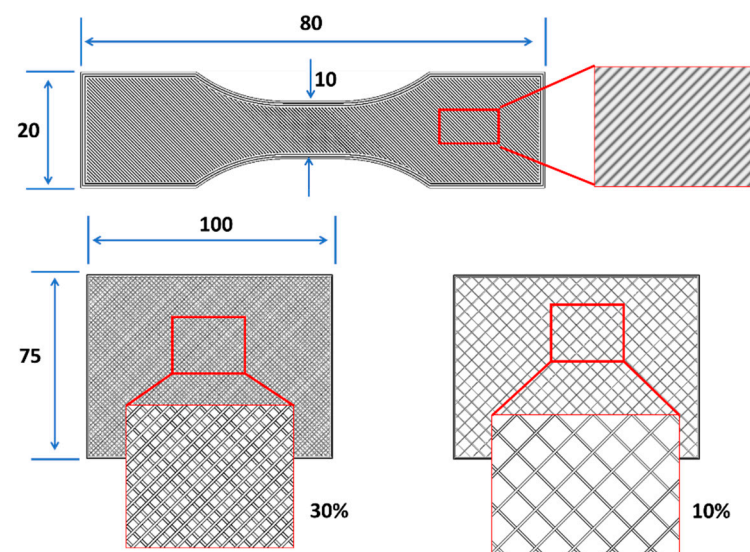


**Figure 2.** Sample dimensions used for PC 3D printing.

The selected layup corresponded to a printing angle (θ) of 0° following the definition reported in [23]. For all 3D printed PC structures, the building direction is aligned with the sample thickness.

Tensile testing experiments were performed using a universal testing machine from Zwick Roell Group (Ulm, Germany) [24]. The machine was equipped with a load cell of 10 kN (Figure 3).
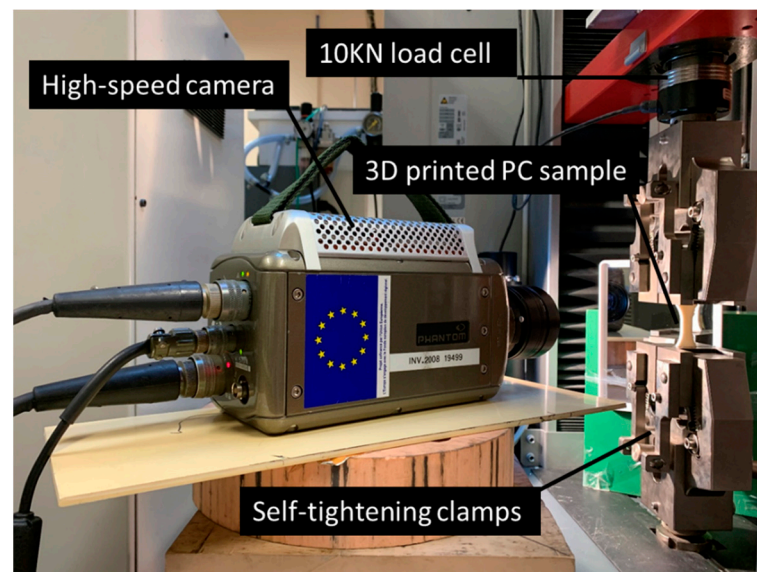


**Figure 3.** Mechanical testing setup.

All tensile experiments were performed using a displacement rate of 5 mm/min up to the sample failure. From the reaction force (*F*)–cross-head displacement (*d*) response, the engineering stress ($\sigma$)–strain ($\varepsilon$) curve was built according to the following conversion

$$\sigma = F/(w \times t) \tag{1}$$

and

$$\varepsilon = d/L_0 \tag{2}$$

where *w*, *t*, and $L_0$ are the width, thickness, and initial length of the specimen at the central part of the specimen, respectively.

Engineering constants were derived from the engineering stress–strain response, namely Young's modulus $E_Y$, yield stress $\sigma_Y$, tensile strength $\sigma_S$, ultimate stress $\sigma_R$, and elongation at break $\varepsilon_R$.

The Young's modulus is derived from the initial slope of the stress–strain curve

$$E_Y = \sigma_e/\varepsilon_e \tag{3}$$

where $\sigma_e$ and $\varepsilon_e$ refer to the engineering stress and strain in the elasticity stage according to Hooke's law.

In the testing setup, a high-speed camera was used to monitor the sample deformation during sample extension. The optical observations were performed using a Phantom V7.3 camera from the Photonline company (Marly Le Roi, 78-France) [22,25]. Both low rate and high rate image recordings were used to observe the entire deformation sequence and achieve higher time resolutions at the rupture point. The frame rate was adjusted accordingly between 100 and 5000 fps (frames per second), and the region of interest (ROI) area was modified between the full frame size (800 × 600 pixels) down to (112 × 320 pixels), with a typical pixel size of 130 μm.

Thermal properties of 3D printed PC samples were assessed using the technique of transient hot probe using the equipment FP2C provided by Neotim company (Albi, France) (Figure 4) according to the ASTM D5930-97 norm [26].
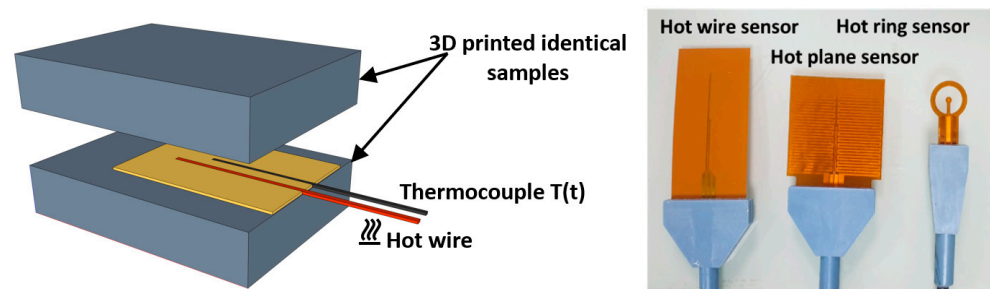
**Figure 4.** Hot probe transient technique with different geometries for thermal properties assessment of 3D printed PC samples.

The equipment was used to measure thermal conductivity, effusivity and diffusivity of PC printed samples from the time evolution of the temperature. The principle consists of local heating of the material using a probe and measuring the temperature increase over time. Thermal properties were assessed by processing the heat signal. Three probes were used (Figure 4). The thermal conductivity was measured using a hot wire probe consisting of a resistive wire and a thermocouple in an insulating Kapton support. The heating power used was 0.14 W. The thermal conductivity was estimated by the equation below:

$$\lambda = \frac{\Phi}{4\pi L \alpha} \tag{4}$$

where $\Phi$ is the linear heat flux, $L$ is the length of the hot wire and $\alpha$ is the slope of the linear part of the thermogram $T(\ln(t))$.

Concerning the thermal effusivity, a hot plane probe was used. The heating power was adjusted to 2.5 W. As for the thermal diffusivity, a hot ring probe was used. The heating time was adjusted to 10 s and the duration of the measurement was, respectively, 60 s and 70 s for PC samples of 10% and 30% of infill rate. The heating power was 3.01 W.

The thermal diffusivity is given by the following expression according to [27]

$$Diff = \frac{r^2}{6} \frac{t_0}{(t_m - t_0) t_m \log\left(\frac{t_m}{t_m - t_0}\right)} \tag{5}$$

where $t_m$ is the time corresponding to the maximum of the temperature by the data of the ring source and r is the radius of the ring.

Two samples of $(7.5 \times 10 \times 2)$ cm were required for each measurement. Figure 4 illustrates the probe geometries used for the measurements.

The thermal conductivity was measured within the range 0.02 à 5 W·m$^{-1}$·K$^{-1}$. The thermal effusivity was measured in the range (20–10,000) J·m$^{-2}$·K$^{-1}$·s$^{-1/2}$ within a temperature interval of $-60\,^{\circ}$C to $100\,^{\circ}$C. The thermal diffusivity measurement range was between 0.1 and 4 mm$^2$·s$^{-1}$. For all thermal properties, the temperature interval used was between $60\,^{\circ}$C and $100\,^{\circ}$C.

## 3. Results and Discussion

Figure 5 compares the tensile response of four as-received PC filaments.

The filament exhibits an elastic–plastic behaviour with a large necking behaviour revealed by optical recording in Figure 6.

Most of the measured engineering quantities (Table 3) are obtained with a small scatter below 6% with the exception of Young's modulus (20%) and elongation at break (16%). Furthermore, the achieved values for Young's modulus and elongation at break are consistent with the data provided by the supplier. The scatter represents only 3% and 2%, respectively.
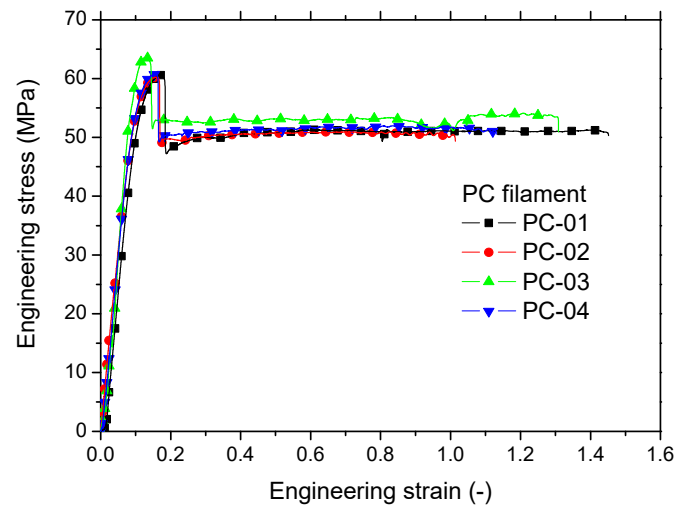
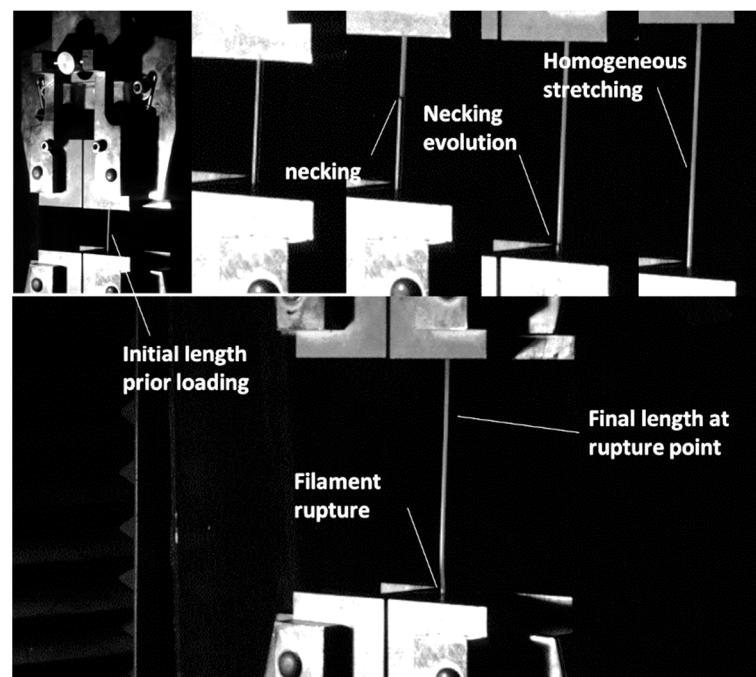**Figure 5.** Typical stress–strain curves of as-received four replicates of PC filament.



**Figure 6.** Stretching stages of PC filament up to rupture point.

**Table 3.** Engineering constants for the as-received PC filament and printed specimens as a function of printing temperature.

| $T_P$ (°C) | $T_B$ (°C) | $E_Y$ (MPa) | $\sigma_Y$ (MPa) | $\sigma_S$ (MPa) | $\sigma_R$ (MPa) | $\varepsilon_R$ (−) |
|---|---|---|---|---|---|---|
| PC filament | | $678 \pm 134$ | $41.9 \pm 2.36$ | $61.3 \pm 1.57$ | $50.3 \pm 0.68$ | $1.23 \pm 0.19$ |
| 270 | 110 | $568 \pm 37$ | $31.5 \pm 4.88$ | $37.2 \pm 4.54$ | $26.6 \pm 14.16$ | $0.09 \pm 0.002$ |
| 280 | 110 | $639 \pm 10$ | $35.5 \pm 0.29$ | $42.9 \pm 0.49$ | $39.0 \pm 0.77$ | $0.08 \pm 0.003$ |
| 290 | 110 | $568 \pm 15$ | $28.0 \pm 0.96$ | $33.9 \pm 0.92$ | $31.9 \pm 2.61$ | $0.07 \pm 0.003$ |
| 300 | 110 | $567 \pm 25$ | $31.6 \pm 0.60$ | $35.5 \pm 1.58$ | $34.8 \pm 1.79$ | $0.07 \pm 0.003$ |

Typical stress–strain response of 3D printed PC is shown in Figure 7 as a function of printing temperature ($T_p$).
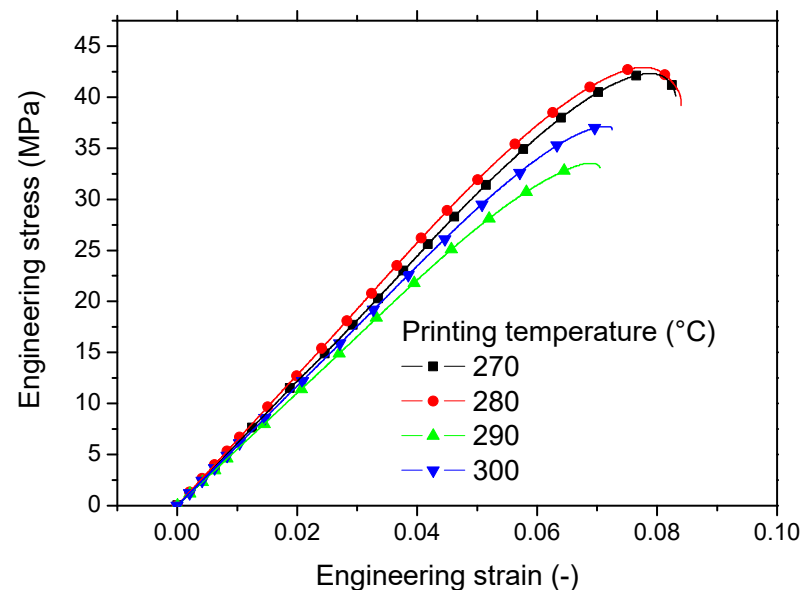
**Figure 7.** Typical stress–strain curves of PC as a function of printing temperature.

A straightforward ranking of the tensile response with the printing temperature $T_P$ is not obtained. The optimal $T_p$ of 280 °C is obtained allowing the 3D printed PC to achieve the highest stiffness and strength. All curves exhibit elastic–plastic behaviour with a minor stretching between strength and ultimate stress. The limited plasticity contrasts with the results obtained for the filament tensile response (Figure 5). Within the considered range of $T_P$, Table 3 summarises the obtained results for all engineering constants including Young's modulus $E_Y$, yield stress $\sigma_Y$, tensile strength $\sigma_S$, ultimate stress $\sigma_R$, and elongation at break $\varepsilon_R$. A large reduction in the elongation at break is experienced when printing the PC with the layups considered. This reduction represents, on average, 71% of the elongation potential of PC. Surprisingly, the loss of stiffness is minor compared to other polymers printed using FDM [28]. It represents less than 10%.

For the remaining engineering quantities, namely yield stress, tensile strength, and ultimate stress, the amount of mechanical loss is within the range of variation reported for FDM, with an average scatter of 17%, 28%, and 24%, respectively.

Figure 8 illustrates the optical recording of tensile response of 3D printed PC structures as a function of printing temperature $T_P$. With the layups of $-45°/+45°$ oriented within the plane of construction, the stretching of the filament arrangement produces a significant deviation with respect to the opening mode at low printing temperatures below 290 °C.

Prior to crack initiation, a change in the grey level of the sample indicates damage initiation, which appears more diffuse with the central area of the specimen.

At higher printing temperatures, the compactness of the filament arrangements restores the opening mode, and unstable cracking takes place leading to a transverse rupture as shown in Figure 8c,d. This tendency toward unstable cracking corresponds to a decrease in the elongation at break (Table 4).

Thermal analysis of 3D printed PC is conducted at the optimal printing temperature ($T_P$ = 280 °C) for which the highest tensile ranking is obtained. Under this condition, two main infill rates are considered as 10% and 30%. Thermal properties are summarized in Table 4, where five replicates are used for each printing condition. High confidence in the results is achieved for all measured quantities. The average scatters for thermal conductivity, effusivity and diffusivity are 1.8%, 3.0%, and 2.4%, respectively.
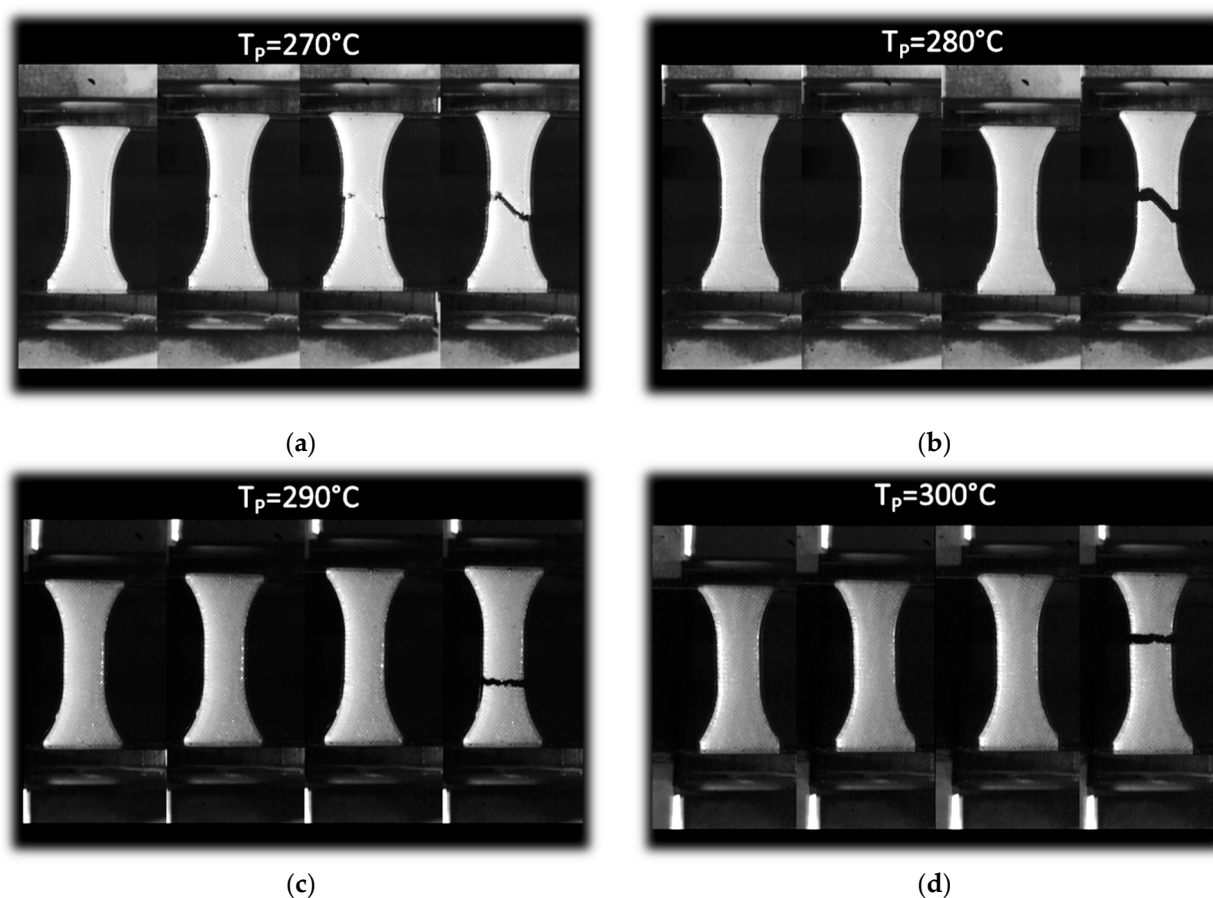
**Figure 8.** Typical optical recording of tensile response of 3D printed PC samples as a function of printing temperature $T_P$: (**a**) 270 °C; (**b**) 280 °C; (**c**) 290 °C; (**d**) 300 °C.

**Table 4.** Thermal properties of 3D printed PC as a function of the in-fill ratio. The printing temperature is 280 °C.

| Infill (%) | Thermal Conductivity (mW/(m/K)) | Thermal Effusivity (W·s$^{0.5}$/(m$^2$·K)) | Thermal Diffusivity ($\times 10^{-7}$ m$^2$/s) |
|---|---|---|---|
| 10 | 54.5 ± 0.75 | 166.8 ± 3.75 | 2.4 + 0.08 |
| 30 | 62.3 ± 1.38 | 234.8 ± 8.75 | 2.0 + 0.03 |

The 3D printed PC material exhibits promising thermal properties with low thermal conductivity and diffusivity and high effusivity. Thermal conductivity and effusivity tend to increase with the infill rate, whereas the thermal diffusivity decreases. The amount of variation for the three properties is 14%, 40%, and 17%, respectively. The 3D printed PC exhibits better thermal properties compared to hemp concrete, for which the thermal conductivity is close to 100 mW/(m·K) [29]. In addition, the effusivity and diffusivity of PC are quite similar to those of hemp concrete which are reported to be between 197 and 256 W·s$^{0.5}$/(m$^2$·K) [30], and between $2 \times 10^{-7}$ and $6 \times 10^{-7}$ m$^2$/s [31,32], respectively. These properties allow the 3D printed PC to achieve good thermal inertia and therefore make it a good insulation material for buildings.

## 4. Conclusions

This study concludes on the high potential of PC material as a candidate for the new generation of insulators in the building sector. Despite the unclear trend of the mechanical performance of 3D printed PC, an optimal printing temperature of 280 °C is obtained. Thermal analysis of 3D printed PC shows that the infill rate has a logical effect on the

thermal conductivity, diffusivity and effusivity, which can be related to the amount of insulating air inside the printed PC. The measured properties demonstrate that PC material is a good candidate for thermal energy storage.

## References

1. Kaynakli, O. A review of the economical and optimum thermal insulation thickness for building applications. *Renew. Sustain. Energy Rev.* **2012**, *16*, 415–425. [CrossRef]
2. Eurostat. *Energy Consumption in Households (EU-28, 2016 Data)*; Eurostat: Luxembourg, 2016.
3. Villasmil, W.; Fischer, L.J.; Worlitschek, J. A review and evaluation of thermal insulation materials and methods for thermal energy storage systems. *Renew. Sustain. Energy Rev.* **2019**, *103*, 71–84. [CrossRef]
4. Aditya, L.; Mahlia, T.M.I.; Rismanchi, B.; Ng, H.M.; Hasan, M.H.; Metselaar, H.S.C.; Muraza, O.; Aditiya, H.B. A review on insulation materials for energy conservation in buildings. *Renew. Sustain. Energy Rev.* **2017**, *73*, 1352–1365. [CrossRef]
5. Mort, R.; Vorst, K.; Curtzwiler, G.; Jiang, S. Biobased foams for thermal insulation: Material selection, processing, modelling, and performance. *RSC Adv.* **2021**, *11*, 4375–4394. [CrossRef] [PubMed]
6. Łach, M. Geopolymer Foams—Will They Ever Become a Viable Alternative to Popular Insulation Materials?—A Critical Opinion. *Materials* **2021**, *14*, 3568. [CrossRef] [PubMed]
7. Belhabib, S.; Guessasma, S. Compression performance of hollow structures: From topology optimisation to design 3D printing. *Int. J. Mech. Sci.* **2017**, *133*, 728–739. [CrossRef]
8. Liu, T.; Guessasma, S.; Zhu, J.; Zhang, W.; Belhabib, S. Functionally graded materials from topology optimisation and stereolithography. *Eur. Polym. J.* **2018**, *108*, 199–211. [CrossRef]
9. Carson, J.K.; Lovatt, S.J.; Tanner, D.J.; Cleland, A.C. An analysis of the influence of material structure on the effective thermal conductivity of theoretical porous materials using finite element simulations. *Int. J. Refrig.* **2003**, *26*, 873–880. [CrossRef]
10. Nazir, A.; Jeng, J.-Y. A high-speed additive manufacturing approach for achieving high printing speed and accuracy. *Proc. Inst. Mech. Eng. Part C J. Mech. Eng. Sci.* **2019**, *234*, 2741–2749. [CrossRef]
11. Löffler, R.; Koch, M. Innovative Extruder Concept for Fast and Efficient Additive Manufacturing. *IFAC-Pap.* **2019**, *52*, 242–247. [CrossRef]
12. Ali, M.H.; Mir-Nasiri, N.; Ko, W.L. Multi-nozzle extrusion system for 3D printer and its control mechanism. *Int. J. Adv. Manuf. Technol.* **2015**, *86*, 999–1010. [CrossRef]
13. Paolini, A.; Kollmannsberger, S.; Rank, E. Additive manufacturing in construction: A review on processes, applications, and digital planning methods. *Addit. Manuf.* **2019**, *30*, 100894. [CrossRef]
14. Vyavahare, S.; Teraiya, S.; Panghal, D.; Kumar, S. Fused deposition modelling: A review. *Rapid Prototyp. J.* **2020**, *26*, 176–201. [CrossRef]
15. Bakır, A.A.; Atik, R.; Özerinç, S. Mechanical properties of thermoplastic parts produced by fused deposition modeling:a review. *Rapid Prototyp. J.* **2021**, *27*, 537–561. [CrossRef]
16. Guessasma, S.; Zhang, W.; Zhu, J.; Belhabib, S.; Nouri, H. Challenges of additive manufacturing technologies from an optimisation perspective. *Int. J. Simul. Multidiscip. Des. Optim.* **2016**, *6*, A9. [CrossRef]
17. Szykiedans, K.; Credo, W. Mechanical Properties of FDM and SLA Low-cost 3-D Prints. *Procedia Eng.* **2016**, *136*, 257–262. [CrossRef]
18. Agron, D.J.S.; Lee, J.-M.; Kim, D.-S. Nozzle Thermal Estimation for Fused Filament Fabricating 3D Printer Using Temporal Convolutional Neural Networks. *Appl. Sci.* **2021**, *11*, 6424. [CrossRef]

19. Vidakis, N.; Petousis, M.; Velidakis, E.; Spiridaki, M.; Kechagias, J.D. Mechanical Performance of Fused Filament Fabricated and 3D-Printed Polycarbonate Polymer and Polycarbonate/Cellulose Nanofiber Nanocomposites. *Fibers* **2021**, *9*, 74. [CrossRef]

20. Gupta, A.; Fidan, I.; Hasanov, S.; Nasirov, A. Processing, mechanical characterization, and micrography of 3D-printed short carbon fiber reinforced polycarbonate polymer matrix composite material. *Int. J. Adv. Manuf. Technol.* **2020**, *107*, 3185–3205. [CrossRef]

21. 3D, V.I. FDM 3D Printers. Available online: https://imprimante-3d-volumic.com/imprimante-3d-francaise/ (accessed on 21 March 2022).

22. Abouzaid, K.; Guessasma, S.; Belhabib, S.; Bassir, D.; Chouaf, A. Printability of co-polyester using fused deposition modelling and related mechanical performance. *Eur. Polym. J.* **2018**, *108*, 262–273. [CrossRef]

23. Guessasma, S.; Belhabib, S.; Nouri, H.; Ben Hassana, O. Anisotropic damage inferred to 3D printed polymers using fused deposition modelling and subject to severe compression. *Eur. Polym. J.* **2016**, *85*, 324–340. [CrossRef]

24. Zwick/Roell. Tensile Testing Machines and Testers. Available online: https://www.zwickroell.com/products/static-materials-testing-machines/universal-testing-machines-for-static-applications/tensile-tester/ (accessed on 21 March 2022).

25. Photonlines. Scientific Cameras. Available online: https://photonlines-recherche.fr/categorie-produit/physique-photonique/cameras-scientifiques/ (accessed on 21 March 2022).

26. *ASTM. D 5930–97*; Standard Test Method for Thermal Conductivity of Plastics by Means of a Transient Line-Source Technique. American Society for Testing and Materials: West Conshohocken, PA, USA, 2009.

27. Marinos, P.G.K.; Tsiambaos, G.C.; Stournaras, H.C. Engineering Geology and the Environment. In Proceedings of the International Symposium on Engineering Geology and the Environmment Greek National Group IAEG, Athens, Greece, 23–27 June 1997; Balkema/Rotterdam/Brookfield: Athens, Greece, 1997.

28. Guessasma, S.; Belhabib, S.; Altin, A. On the Tensile Behaviour of Bio-Sourced 3D-Printed Structures from a Microstructural Perspective. *Polymers* **2020**, *12*, 1060. [CrossRef] [PubMed]

29. Benmahiddine, F.; Bennai, F.; Cherif, R.; Belarbi, R.; Tahakourt, A.; Abahri, K. Experimental investigation on the influence of immersion/drying cycles on the hygrothermal and mechanical properties of hemp concrete. *J. Build. Eng.* **2020**, *32*, 101758. [CrossRef]

30. Seng, B.; Magniont, C.; Lorente, S. Characterization of a precast hemp concrete. Part I: Physical and thermal properties. *J. Build. Eng.* **2019**, *24*, 100540. [CrossRef]

31. Mazhoud, B.; Collet, F.; Pretot, S.; Chamoin, J. Hygric and thermal properties of hemp-lime plasters. *Build. Environ.* **2016**, *96*, 206–216. [CrossRef]

32. Gourlay, E.; Glé, P.; Marceau, S.; Foy, C.; Moscardelli, S. Effect of water content on the acoustical and thermal properties of hemp concretes. *Constr. Build. Mater.* **2017**, *139*, 513–523. [CrossRef]